Bioorganic & Medicinal Chemistry 18 (2010) 5835–5844

Contents lists available at ScienceDirect

Bioorganic & Medicinal Chemistry

journal homepage: www.elsevier.com/locate/bmc

NMR spectroscopy and computational analysis of interaction between *Serratia marcescens* chitinase B and a dipeptide derived from natural-product cyclopentapeptide chitinase inhibitor argifin

Hiroaki Gouda [a,*], Toshiaki Sunazuka [b], Tomoyasu Hirose [b], Kanami Iguchi [b], Noriyuki Yamaotsu [a], Akihiro Sugawara [b], Yoshihiko Noguchi [b], Yoshifumi Saito [b], Tsuyoshi Yamamoto [b], Takeshi Watanabe [c], Kazuro Shiomi [b], Satoshi Ōmura [b], Shuichi Hirono [a]

[a] *School of Pharmacy, Kitasato University, 5-9-1 Shirokane, Minato-ku, Tokyo 108-8641, Japan*
[b] *Kitasato Institute for Life Sciences, Graduate School of Infection Control Science, School of Pharmaceutical Sciences, Kitasato University, 5-9-1 Shirokane, Minato-ku, Tokyo 108-8641, Japan*
[c] *Department of Applied Biological Chemistry, Faculty of Agriculture, Niigata University, 8050 Ikarashi-2, Niigata 950-2181, Japan*

ARTICLE INFO

Article history:
Received 28 May 2010
Revised 25 June 2010
Accepted 29 June 2010
Available online 1 July 2010

Keywords:
Binding free energy
Chitinase
Docking
Molecular dynamics
NMR

ABSTRACT

The dipeptide *N*-acetyl-Arg{N^{ω}-(*N*-methylcarbamoyl)}-*N*-methyl-Phe(**2**), which is a part of the natural-product cyclopentapeptide chitinase inhibitor argifin (**1**), inhibits chitinase B from *Serratia marcescens* (*Sm*ChiB) with a half-maximal inhibitory concentration (IC_{50}) of 3.7 μM. Despite the relatively small size of **2**, its inhibitory activity is comparable with that of **1** (IC_{50} = 6.4 μM). To elucidate the basis for this interesting phenomenon, we investigated the interaction between **2** and *Sm*ChiB using a combination of nuclear magnetic resonance spectroscopy and computational methods. The transferred nuclear Overhauser effect (TRNOE) experiment obtained structural information on the *Sm*ChiB-bound conformation of **2**. The binding mode of **2** and *Sm*ChiB was modeled by the novel molecular-docking approach proposed in our laboratory, which can explicitly consider water-mediated hydrogen-bonding interactions in protein-ligand interfaces. The *Sm*ChiB-bound conformation of **2** in the resulting model satisfied all proton-proton distance constraints derived from the TRNOE experiment, indicating that our model structure of the **2**-*Sm*ChiB complex is reasonable. A molecular dynamics (MD) simulation examined the stability of the resultant complex structure and suggested that **2** binds to *Sm*ChiB in a similar fashion to the binding mode observed for N^{ω}-(*N*-methylcarbamoyl)-Arg(1) and *N*-methyl-Phe(2) of **1** in the crystal structure of the argifin–*Sm*ChiB complex. Finally, the binding free energies of **1** and **2** with *Sm*ChiB were estimated by the molecular mechanics Poisson–Boltzmann surface area (MM-PBSA) method using the MD trajectory. The MM-PBSA calculation suggested that both **1** and **2** bind to *Sm*ChiB with similar affinities, which is consistent with their experimental IC_{50} values. Energetic analysis revealed that the van der Waals interaction of **2** with *Sm*ChiB is much less than that of **1**, but is completely compensated by the more favorable contribution of solute entropy and the total electrostatic component. The improved total electrostatic component was derived from more favorable electrostatic interactions. Therefore, we conclude that dipeptide **2** was also better optimized against *Sm*ChiB than **1** in an electrostatic point of view.

1. Introduction

Family 18 chitinases catalyze the hydrolysis of chitin, which is a linear polymer of β-(1,4)-linked *N*-acetyl-D-glucosamine (GlcNAc) and is one of the most abundant biopolymers in nature. These enzymes are present in a wide range of organisms including bacteria, fungi, insects and mammals, including humans.[1–5] As chitin is a major structural component of fungi and insects, family 18 chitinases play important physiological roles in these organisms.[2,3,6,7] Mammalian acidic chitinase has also been implicated in triggering asthma.[8] Therefore, chitinase inhibitors have attractive potential to function as fungicides, insecticides and anti-asthma medications.[9–11] Nevertheless, no practical use for chitinase inhibitors has been developed to date.

During screening for chitinase inhibitors in our laboratory, the novel cyclic pentapeptide argifin (**1**) was isolated from the culture

Abbreviations: GlcNAc, *N*-acetyl-D-glucosamine; MD, molecular dynamics; MM-PBSA, molecular mechanics Poisson–Boltzmann surface area; TRNOE, transferred nuclear Overhauser effect.

* Corresponding author. Tel.: +81 3 3444 3548; fax: +81 3 3440 5246.
E-mail address: godah@pharm.kitasato-u.ac.jp (H. Gouda).

0968-0896/$ - see front matter © 2010 Elsevier Ltd. All rights reserved.
doi:10.1016/j.bmc.2010.06.093

broth of *Gliocladium* sp. FTD-0668 (Fig. 1).[12] Its potent inhibitory activity against chitinases[12,13] and the recent establishment of total synthesis strategies, independently established by Eggleston and co-workers and our groups,[14,15] suggest that it might be useful as a candidate for the development of novel drugs. The three-dimensional (3D) structure of **1**, in complex with chitinase B from *Serratia marcescens* (*Sm*ChiB), was also resolved by X-ray crystallography.[16] **1** inhibits *Sm*ChiB with a half-maximal inhibitory concentration (IC_{50}) value of 6.4 μM.[15]

These observations led us to study the structure-activity relationship (SAR) between **1** and *Sm*ChiB. In our previous SAR study[15] on acyclic analogs of **1**, we found that the dipeptide *N*-acetyl-Arg{N^{ω}-(*N*-methylcarbamoyl)}-*N*-methyl-Phe(**2**), which corresponds to N^{ω}-(*N*-methylcarbamoyl)-Arg(1) and *N*-methyl-Phe(2) of **1** (Fig. 1), exhibits a half-maximal inhibitory concentration (IC_{50}) of 3.7 μM for *Sm*ChiB. As **2** is much smaller than **1**, this is an interesting result. Therefore, we performed interaction analysis between **2** and *Sm*ChiB using a combination of nuclear magnetic resonance (NMR) spectroscopy and computational methods. Initially, we obtained interproton distance constraints for the *Sm*ChiB-bound conformation of **2** using the transferred nuclear Overhauser effect (TRNOE) experiment.[17–19] Then, the binding mode of **2** with *Sm*ChiB was modeled using the novel molecular-docking approach proposed in our laboratory,[20] which can explicitly consider water molecules forming hydrogen-bond bridges between proteins and ligands. The resulting binding mode was validated using distance constraints derived from the TRNOE experiment. Finally, the binding affinities of **1** and **2** with *Sm*ChiB were estimated by applying the molecular mechanics Poisson–Boltzmann surface area (MM-PBSA) method[21] combined with the molecular dynamics (MD) simulation. The energetic analysis revealed the basis for **2** to possess the potent inhibitory activity compared with **1**.

2. Results and discussion

2.1. TRNOE experiment

The TRNOE experiment is widely used to analyze conformations of ligands bound to large proteins.[17–19] It offers the advantage over other NMR methods and X-ray crystallography in that it does not require large amounts of proteins or expensive isotopic labeling. In this study, we performed the TRNOE experiment to obtain structural information about the *Sm*ChiB-bound conformation of **2**, which is used to validate the complex structure of **2** with *Sm*ChiB modeled in the following computational analysis.

The ^{1}H resonance assignments of **2** in aqueous solution were first made by DQF-COSY,[22] TOCSY[23] and ROESY[24] experiments. We found that **2** gave two different sets of resonances in an approximate 4:5 ratio, due to the presence of *cis*- and *trans*-configurations of the amide bond between N^{ω}-(*N*-methylcarbamoyl)-Arg(1) and *N*-methyl-Phe(2). The resonance assignments of **2** are given for both *trans*- and *cis*-configurations in Supplementary Table 1. Next, the 1D spectra of **2** were compared in the absence and presence of *Sm*ChiB (Fig. 2). Interestingly, only the resonances for the *cis*-configuration of **2** were selectively broadened in the presence of *Sm*ChiB, suggesting that *Sm*ChiB binding is *cis*-configuration-specific.

The 2D-NOESY[25] spectra of **2** were then recorded in the absence and presence of *Sm*ChiB. The 2D-NOESY spectra of **2** in its free state provided only a few cross-peaks with the opposite sign to diagonal resonances. These cross-peaks are due to positive proton-proton

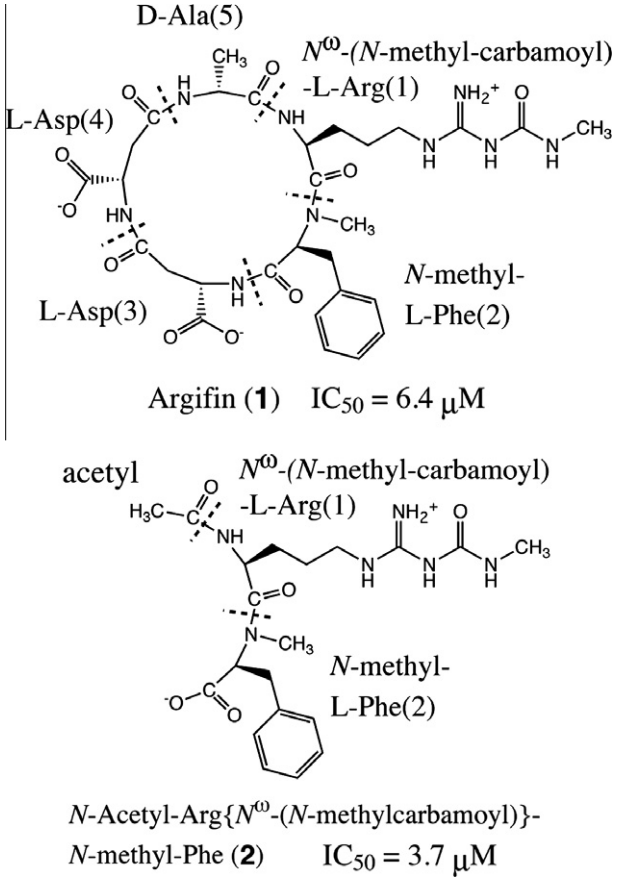

Figure 1. Chemical structures and IC_{50} values against *Sm*ChiB of argifin (**1**) and dipeptide (**2**).

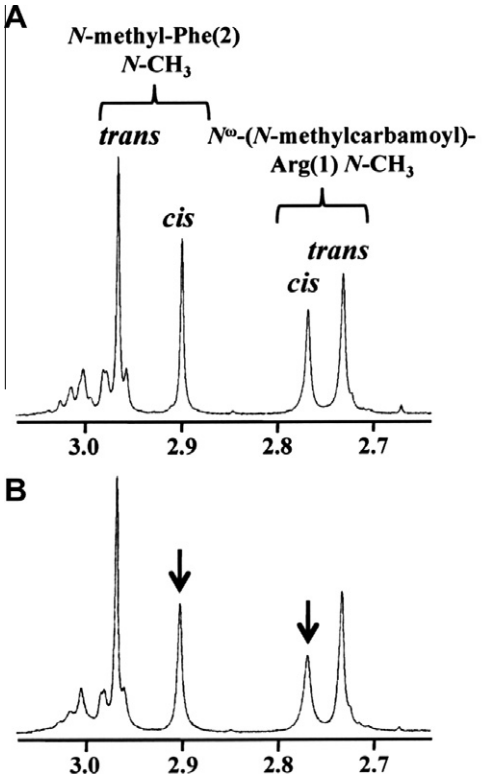

Figure 2. (A) 1D ^{1}H NMR spectrum of dipeptide **2** in the absence of *Sm*ChiB. (B) 1D ^{1}H NMR spectrum of dipeptide **2** in the presence of *Sm*ChiB. Addition of *Sm*ChiB selectively broadened resonances from molecule with *cis*-configuration of amide bond between N^{ω}-(*N*-methylcarbamoyl)-Arg(1) and *N*-methyl-Phe(2) (arrows).

NOEs, indicating a fast correlation time for **2** in the free state ($\tau_c < 10^{-10}$ s). On the other hand, the 2D-NOESY spectrum of **2** in the presence of *Sm*ChiB is shown in Figure 3. Interestingly, we only observed negative NOE cross-peaks with the same sign as the diagonal resonances for **2** in the *cis*-configuration (Fig. 3). These negative NOEs (TRNOEs) clearly confirmed that only the molecule with *cis*-configuration binds with *Sm*ChiB. The intensities of these TRNOEs were calculated to extract interproton distance constraints on the *Sm*ChiB-bound conformation of **2**. As the NOE cross-peak intensity is approximately proportional to the inverse sixth power of the interproton distance, we could quantitatively classify the observed TRNOE data into three distance ranges, 1.8–3.0, 1.8–4.0 and 1.8–5.0 Å, corresponding to strong, medium, and weak TRNOEs, respectively. A total of 13 distance constraints were obtained as shown in Table 1. These constraints were used to validate the complex structure of **2** with *Sm*ChiB modeled in the following computational analysis.

A strong TRNOE was observed between Hα protons of N^{ω}-(*N*-methylcarbamoyl)-Arg(1) and *N*-methyl-Phe(2) of **2** (Fig. 3 and Table 1), indicating that the *cis*-configuration between these two residues is retained even in the *Sm*ChiB-bound conformation. Importantly, two TRNOEs were observed between the aliphatic protons of N^{ω}-(*N*-methylcarbamoyl)-Arg(1) and the benzyl protons of *N*-methyl-Phe(2) (Table 1). This result suggests that the side chains of these two residues pack tightly together in the *Sm*ChiB-bound conformation of **2**.

2.2. Modeling of binding mode of 2 with SmChiB

Figure 4A shows the binding mode observed in the crystal structure of the argifin–*Sm*ChiB complex.[16] Argifin (**1**) used N^{ω}-(*N*-methylcarbamoyl)-Arg(1) and Asp(3) to form a total of five direct hydrogen-bonds with W97, D142, E144, and Y214 of *Sm*ChiB. An aromatic stacking interaction between the *N*-methyl-Phe(2) of **1** and W97, Y145, F191 and W220 of *Sm*ChiB was also observed. Importantly, a total of six water molecules were suggested to form hydrogen-bonding bridges between **1** and *Sm*ChiB (Fig. 4A).[16] These water molecules may be important both in allowing *Sm*ChiB to recognize **1** and in stabilizing the complex structure. In particular, the region of N^{ω}-(*N*-methylcarbamoyl)-Arg(1) and *N*-methyl-Phe(2) of **1**, which corresponds to dipeptide **2**, is related to two water-mediated hydrogen-bonding interactions with *Sm*ChiB (Fig. 4A).

Based on these observations, we consider that the binding of **2** with *Sm*ChiB might also require such water-mediated interactions. Therefore, we modeled the binding mode of **2** with *Sm*ChiB using the novel molecular-docking procedure proposed recently in our laboratory.[20] This procedure includes the docking calculation using hypothetically hydrated ligand molecules, which are prepared by connecting ligand hydrogen-bonding functional groups with water molecules through a hypothetical bond of 2.7 Å (a typical distance for hydrogen bonding).[20] Therefore, it can explicitly consider water molecules forming hydrogen-bond bridges between proteins and ligands. The details are described in Section 4. Our previous study showed that this novel approach could reproduce the binding modes including water-mediated hydrogen-bonding interactions determined crystallographically.[20]

The resulting binding model of dipeptide **2** with *Sm*ChiB is shown in Figure 4B. First, we confirmed that the binding conformation of **2** in this model satisfied all structural information derived from the TRNOE experiment. For example, our procedure could select the binding mode where **2** adopted *cis*-configurations of the amide bond between N^{ω}-(*N*-methylcarbamoyl)-Arg(1) and *N*-methyl-Phe(2), although both *cis*- and *trans*-configurations were observed in the generated poses (see Supplementary Table 2). Therefore, our binding model of **2** with *Sm*ChiB was strongly suggested to be reasonable. We note that the docking calculation using only a native structure of dipeptide **2** without incorporating water molecules could not generate docking poses satisfying all experimental constraints, indicating that our procedure was useful for investigating the binding mode of **2** with *Sm*ChiB.

The orientation of **2** within the ligand binding-site of *Sm*ChiB is visually similar to that of the region of N^{ω}-(*N*-methylcarbamoyl)-Arg(1) and *N*-methyl-Phe(2) of **1** (Fig. 4A and B). Therefore, **2**

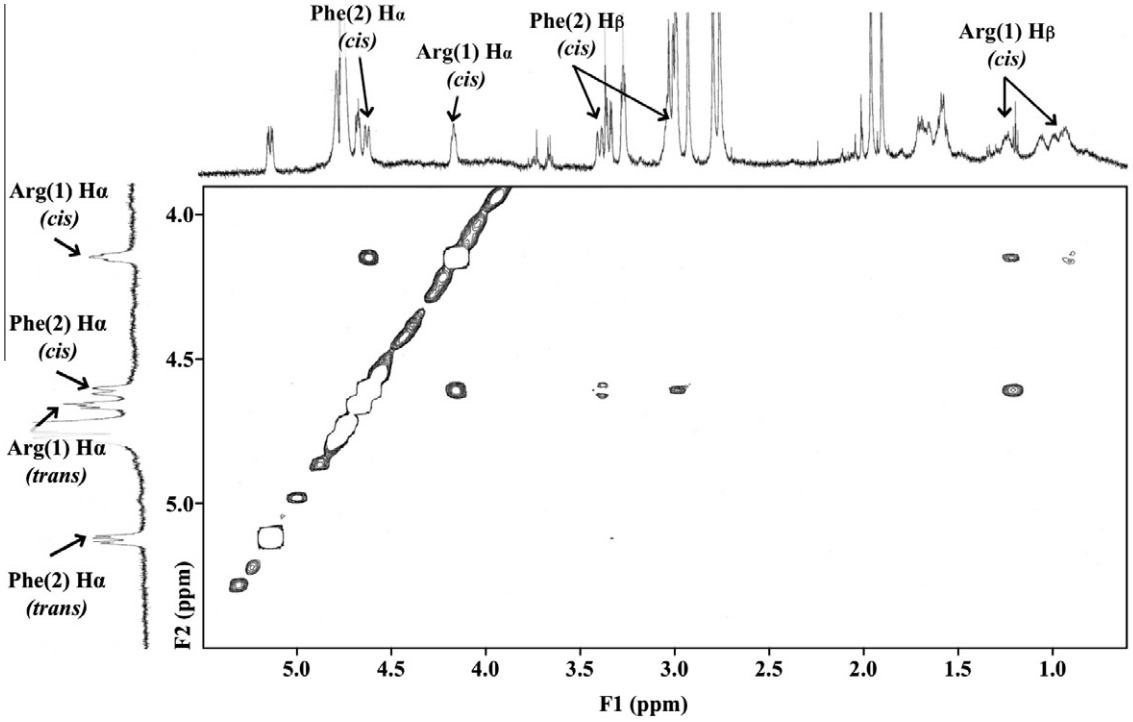

Figure 3. 2D NOESY spectrum of dipeptide **2** in the presence of *Sm*ChiB using a 200-ms mixing time. Only cross-peaks with same sign as diagonal resonances are displayed.

Table 1
Distance constraints obtained by the TRNOE experiment of dipeptide **2**

Atom A		Atom B		Upper bound (Å)
Arg(1)	Hα	Arg(1)	Hβ (0.90 ppm)	4.0
Arg(1)	Hα	Arg(1)	Hβ (1.22 ppm)	3.0
Arg(1)	Hβ (0.90 ppm)	Arg(1)	Hδ	4.0
Arg(1)	Hα	*N*-Methyl-Phe(2)	Hα	3.0
Arg(1)	Hβ (1.22 ppm)	*N*-Methyl-Phe(2)	Hα	3.0
Arg(1)	Hβ (1.22 ppm)	*N*-Methyl-Phe(2)	Hδ	5.0
Arg(1)	Hδ	*N*-Methyl-Phe(2)	Hε	4.0
N-Methyl-Phe(2)	*N*-CH_3	*N*-Methyl-Phe(2)	Hδ	3.0
N-Methyl-Phe(2)	Hα	*N*-Methyl-Phe(2)	Hβ (2.96 ppm)	3.0
N-Methyl-Phe(2)	Hα	*N*-Methyl-Phe(2)	Hβ (3.38 ppm)	4.0
N-Methyl-Phe(2)	Hα	*N*-Methyl-Phe(2)	Hδ	4.0
N-Methyl-Phe(2)	Hβ (2.96 ppm)	*N*-Methyl-Phe(2)	Hδ	3.0
N-Methyl-Phe(2)	Hβ (3.38 ppm)	*N*-Methyl-Phe(2)	Hδ	3.0

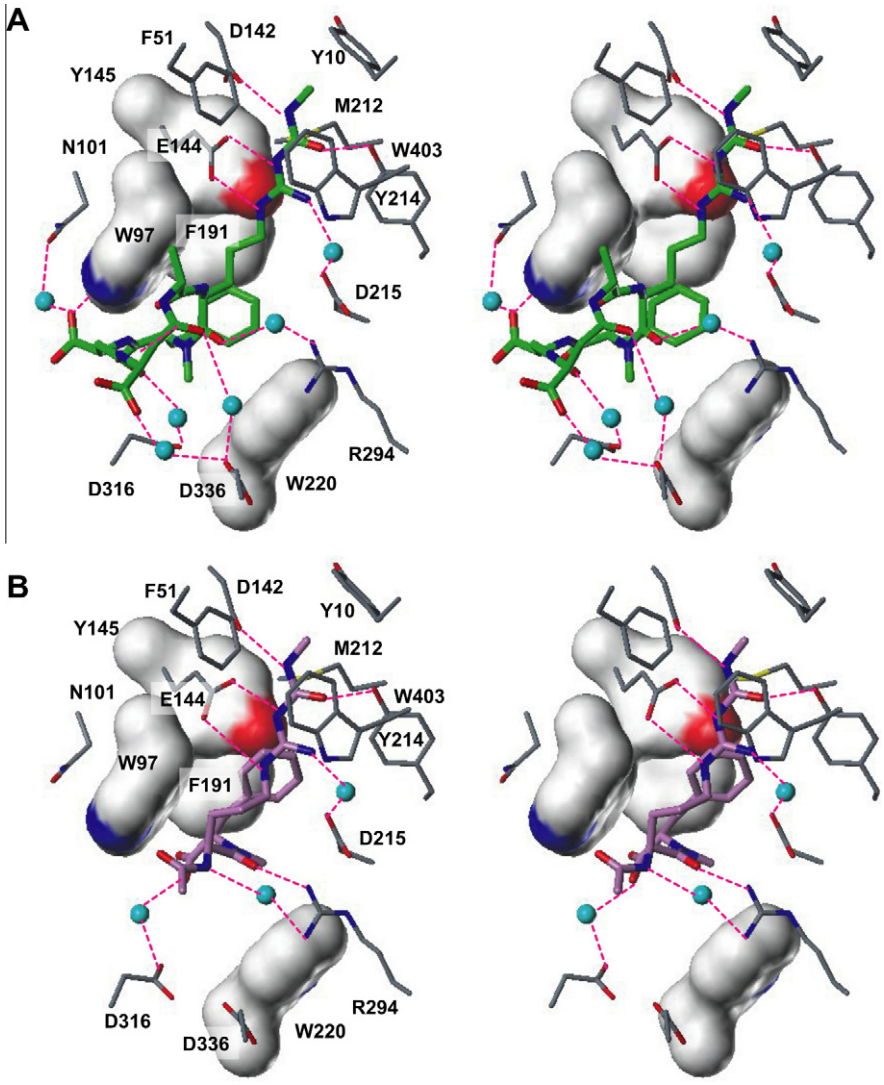

Figure 4. (A) Stereoview of binding mode of argifin with *Sm*ChiB determined crystallographically. (B) Stereoview of binding mode of dipeptide **2** with *Sm*ChiB determined by our docking procedure. Hydrogen-bonding interactions are indicated by red dashed lines. Cyan spheres represent water molecules potentially forming hydrogen-bonding bridges between ligand and *Sm*ChiB.

formed four direct hydrogen-bonds with D142, E144 and Y214 of *Sm*ChiB, as observed in the crystal structure of the argifin–*Sm*ChiB complex. Unlike **1**, **2** did not make a direct hydrogen-bond with W97 of *Sm*ChiB, however it formed an alternative one with R294 using a backbone oxygen atom of N^{ω}-(*N*-methylcarbamoyl)-Arg(1) (Fig. 4B). As a result, the number of direct hydrogen-bonds in the **2**–*Sm*ChiB complex was the same as in the argifin–*Sm*ChiB complex. The *N*-methyl-Phe(2) of **2** was located in the hydrophobic pocket formed by W97, Y145, F191 and W220 of *Sm*ChiB, similar to **1**, although its location was shifted toward Y145.

In our model of the dipeptide **2**–*Sm*ChiB complex, a total of three water-mediated hydrogen-bonding interactions were suggested (Fig. 4B). A water molecule between the $N_{\eta 2}$ atom of N^{ω}-(*N*-methylcarbamoyl)-Arg(1) and D215 of *Sm*ChiB, observed in the crystal structure of the argifin–*Sm*ChiB complex, was conserved in the binding mode of **2** with *Sm*ChiB. Two further water-mediated interactions were formed between the backbone N atom of N^{ω}-(*N*-methylcarbamoyl)-Arg(1) and R294 and between the carbonyl O atom of the C-terminal and D316. Both R294 and D316 of *Sm*ChiB were also related to the water-mediated interactions in the argifin–*Sm*ChiB complex, although their partner atoms in **1** were different from those in **2**.

The molecular dynamics (MD) simulation in a box of water molecules was performed to examine the stability of the resultant structure of the **2**–*Sm*ChiB complex. The 2000 ps MD simulation was performed using the AMBER8.0 package and the Cornell et al. force field.[26,27] The RMSD values relative to the initial structure were monitored along the entire MD trajectory. We calculated RMSD values for the whole and for the subregions, that is, the catalytic domain with dipeptide **2** and the C-terminal domain. These values of the catalytic and C-terminal domains almost reached a stable state after about 1000 ps, and nearly converged (see Supplementary Fig. 1). However, the RMSD on the whole fluctuated between 1.5 and 3.0 Å, which was due to interdomain motion via the flexible linker between these two domains as observed in the MD simulation of the argifin–*Sm*ChiB complex in our previous study.[28] Therefore, a total of 100 snapshots with an interval of 10 ps from the last 1000 ps trajectory was considered for an ensemble of solution structures, and used for our subsequent hydrogen-bonding analysis. For comparison, the ensemble of solution structures for the argifin–*Sm*ChiB complex was also prepared from the MD trajectory obtained in our previous study.[28]

Figure 5 shows a comparison of the final MD structure between the argifin–*Sm*ChiB complex and the dipeptide **2**–*Sm*ChiB complex. The MD simulation could relax the dipeptide **2**–*Sm*ChiB complex to move the *N*-methyl-Phe(2) of **2** into the same position as observed in the argifin–*Sm*ChiB complex (Fig. 5A and B). Thus, the MD simulation was useful to refine the local structure. Hydrogen-bonding analysis over the MD trajectory showed that the five direct hydrogen-bonds between **2** and *Sm*ChiB were as stable as those in the argifin–*Sm*ChiB complex (Table 2). This suggests that the binding model of **2** was relatively stable, implying that **2** is highly likely to bind to *Sm*ChiB with the interaction mode shown in Figure 5B. In the MD simulation, an additional direct hydrogen-bond was formed between the $N_{\eta 2}$ atom of N^{ω}-(*N*-methylcarbamoyl)-Arg(1) of **2** and D215 with a high occupancy (about 95%), as shown in Table 2B.

In the docking model, a water-mediated hydrogen-bonding interaction was observed between these two atoms (Fig. 4B), of which occupancy was about 5% over the MD trajectory (Table 2B). The sum of these two occupancy values approached 100%. These results indicate that there was a dynamic transition between direct (major) and water-mediated (minor) hydrogen-bonding formations for this interaction site. The *Sm*ChiB template structure for docking was extracted from the crystal structure of the argifin–*Sm*ChiB complex, in which D215 of *Sm*ChiB was related to a water-mediated interaction with **1** (Fig. 4A). Therefore, the observation of minor interaction in the docking model of **2** is probably due to the disposition of D215 in the *Sm*ChiB template structure. Interestingly, a similar dynamic interaction was also observed between the $N_{\eta 2}$ atom of N^{ω}-(*N*-methylcarbamoyl)-Arg(1) of **1** and D215 in the MD trajectory of the argifin–*Sm*ChiB complex (Table 2A). The water-mediated hydrogen-bonding between the backbone N atom of N^{ω}-(*N*-methylcarbamoyl)-Arg(1) of **2** and R294 also showed a relatively low occupancy of 7% (Table 2B), as the N-terminal region of **2** was found to be flexible in the MD trajectory. These two water-mediated interactions described above seem to be temporary and less important for the binding of **2** with *Sm*ChiB.

By contrast, the water-mediated hydrogen-bonding bridges between the C-terminal carbonyl O atom of **2** and D316 showed very high occupancy of 84% (Table 2B). Moreover, we found that an average of two water molecules were involved in this interaction site (Fig. 5B and Supplementary Fig. 2), although they were frequently replaced with bulk molecules. These results indicate that this water-mediated interaction is important for the binding of **2** with *Sm*ChiB. The water molecules probably play an important role in shield effects on the unfavorable electrostatic interaction between the C-terminal carbonyl O atom of **2** and D316. In the MD trajectory of the argifin–*Sm*ChiB complex, three of six water-mediated interactions observed in the crystal structure showed high occupancies (>60%), indicating their importance in the binding of **1** with *Sm*ChiB (Fig. 5A and Table 2A).

Overall, dipeptide **2** is likely to bind to *Sm*ChiB in a very similar fashion to the binding mode observed for N^{ω}-(*N*-methylcarbamoyl)-Arg(1) and *N*-methyl-Phe(2) of **1**, although there are a few differences, such as the number of water-mediated interactions. Therefore, we were unable to clearly explain the basis for **2** to possess potent activity compared with **1** from a structural point of view. In the following, we performed binding free energy calculations to examine the energetic basis.

2.3. Estimation of binding free energy by the MM-PBSA method using the MD trajectory

In the general MM-PBSA method, the absolute binding free energy is defined as follows:

$$\Delta G_{\text{bind}} = G_{\text{complex}} - (G_{\text{free protein}} + G_{\text{free ligand}}). \quad (1)$$

Here, G_{complex}, $G_{\text{free protein}}$, and $G_{\text{free ligand}}$ are the free energies of the complex, the free protein, and the free ligand, respectively.[21] In our calculations, we used the following approximation:

$$G_{\text{free protein}} \approx G_{\text{bound protein}}. \quad (2)$$

This assumes that the protein conformations are similar in both bound and free states. With respect to this approximation, we used the crystal structures of the argifin–*Sm*ChiB complex (PDB:1H0I) and *Sm*ChiB in the free state (PDB:1E15) to calculate the RMSD between the free *Sm*ChiB and the argifin–bound *Sm*ChiB with a total of 37 residues surrounding the binding site. The calculated RMSD value of 1.01 Å was relatively small, indicating that the binding site structure of the free *Sm*ChiB was similar to that of argifin–bound *Sm*ChiB. Therefore, we assumed that the approximation of Eq. 2 was adequate for the binding of dipeptide **2** as well as **1** to *Sm*ChiB, that is, the coordinates for unbound *Sm*ChiB were taken from the complex trajectory to estimate $G_{\text{free protein}}$ ($\approx G_{\text{bound protein}}$). The estimation of binding free energies using this approximation has been successfully performed for a variety of protein–ligand,[29–33] RNA–ligand,[34] and DNA–ligand[35] interactions.

On the other hand, the unbound conformations of **1** and dipeptide **2** were obtained from separate MD trajectories of the ligand free in solution. For dipeptide **2** in the free state, two MD simulations were performed, one for the *cis*-configuration of the amide bond between N^{ω}-(*N*-methylcarbamoyl)-Arg(1) and *N*-methyl-Phe(2) and the other for *trans*-configuration. $G_{\text{free ligand}}$ of **2** was estimated using the unbound conformations derived from these two MD simulations in the weighted-average manner according to the ratio from the NMR experiments. As observed earlier, two water molecules in the dipeptide **2**–*Sm*ChiB complex and three in the argifin–*Sm*ChiB complex involved in the hydrogen bonding bridges with high occupancies seem to play an important role in forming and stabilizing their structures. Therefore, these water molecules were explicitly considered as part of the protein.

The results are summarized in Table 3. The calculated ΔG_{bind} values were −6.32 and −6.30 kcal/mol for the dipeptide **2**–*Sm*ChiB

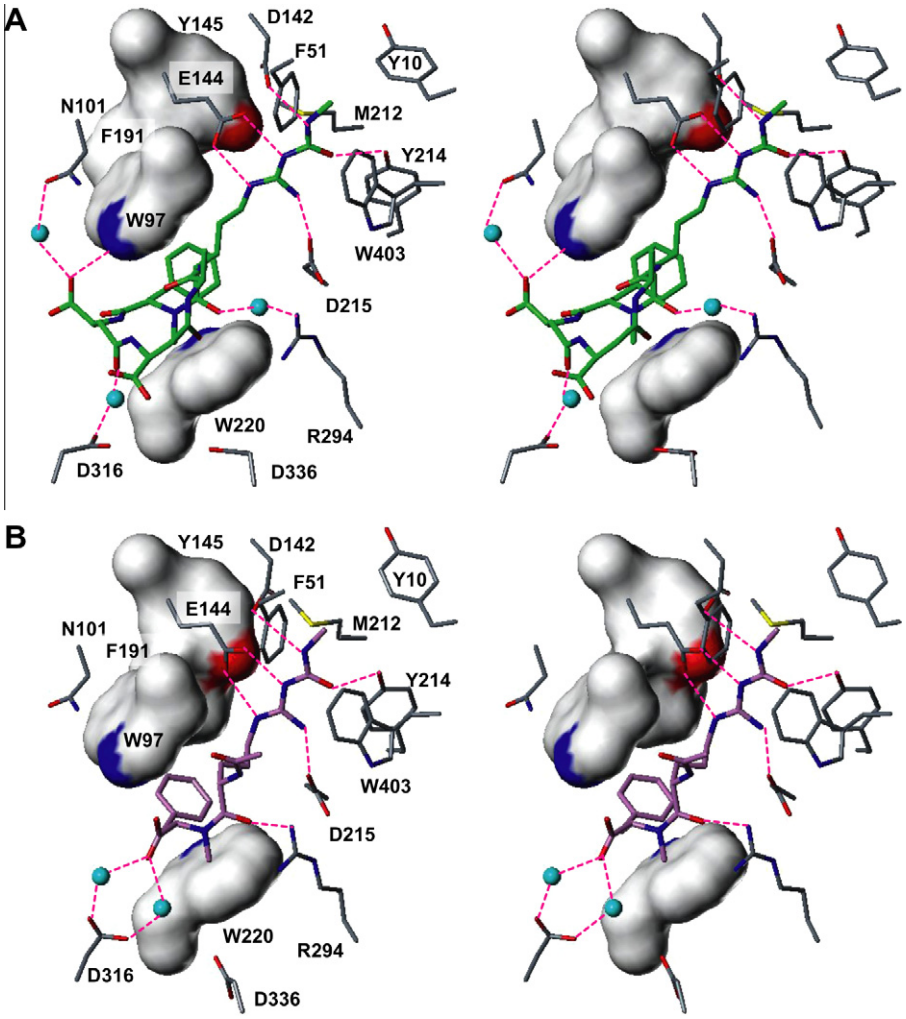

Figure 5. (A) Stereoview of final MD structure of argifin–*Sm*ChiB complex. (B) Stereoview of final MD structure of dipeptide **2**–*Sm*ChiB complex. Hydrogen-bonding interactions are indicated by red dashed lines. Only water molecules forming hydrogen-bonding bridges with high occupancy over MD trajectory are included.

and argifin–*Sm*ChiB complexes, respectively. The ΔG_{bind} value (−6.30 kcal/mol) for the argifin–*Sm*ChiB complex was in very good agreement with that derived from the experimental inhibition constant value (−6.36 kcal/mol) reported by Eggleston and coworkers,[16] indicating that the MM-PBSA method considering water-mediated interactions can accurately reproduce absolute binding free energies. In our previous MM-PBSA study without analysis of water-mediated interactions, we obtained a ΔG_{bind} value of −6.98 kcal/mol for the binding of **1** with *Sm*ChiB.[28] The comparison suggested that the consideration of water-mediated interactions in protein–ligand interfaces could provide a small but significant improvement for the calculation of ΔG_{bind} value. The importance of considering water-mediated interactions in the MM-PBSA method has also been reported in several studies.[33–35]

As shown in Table 3, the MM-PBSA calculations suggested that both **2** and **1** bind to *Sm*ChiB with similar affinities. This result is consistent with the observation that both dipeptide **2** and **1** possess almost identical IC_{50} values against *Sm*ChiB (Fig. 1 and Table 3). Therefore, we compared the contributions to binding between dipeptide **2** and **1** to examine the basis for **2** to possess potent activity compared with **1**. The van der Waals and nonpolar solvation energies of dipeptide **2** were less favorable than that of **1**, as expected from its smaller size. However, these losses were completely compensated by the more favorable contributions of solute entropy and total electrostatic component ($\Delta G_{elec+PB}$) of **2**. As a result, calculated ΔG_{bind} values were almost the same between dipeptide **2** and **1**.

Normal mode analysis indicated that the binding of **2** leads to a less tightening of the complex structure and, hence, a more favorable contribution from the solute entropy when compared with that of **1**. In other words, the change in vibrational entropy upon binding is smaller in the **2**–*Sm*ChiB complex. The total electrostatic component of the binding free energy ($\Delta G_{elec+PB}$) is the sum of the electrostatic interaction energy (ΔE_{elec}) and the electrostatic term in the solvation energy (ΔG_{PB}). As shown in Table 3, the much greater electrostatic interaction of **2** with *Sm*ChiB led to the more favorable contributions of the total electrostatic component. Therefore, we could consider that the more favorable electrostatic interactions are significantly responsible for **2** to possess potent activity compared with **1**. Accordingly, the electrostatic interaction energies between individual residues of *Sm*ChiB and dipeptide **2** (argifin) were calculated to determine which residues of *Sm*ChiB make an important contribution to the differential in the electrostatic interaction.

Figure 6 shows the subtraction between the electrostatic interaction energies of the dipeptide **2**–*Sm*ChiB complex and those of the argifin–*Sm*ChiB complex. Residues with negative and positive differences have more favorable electrostatic interaction energies with **2** and **1**, respectively. In total, there were seven residues with an absolute difference larger than 10.0 kcal/mol, five of which (D102, E315, D316, D334, and D336) possessed increased electro-

Table 2
Hydrogen-bonding interactions observed in the MD trajectory of complexes

Argifin	*Sm*ChiB	% Occupied
A: Argifin–*Sm*ChiB complex		
Direct H-bonding interactions between argifin and SmChiB		
Methyl-carbamoyl N	D142 $O_{\delta 2}$	72.0
Methyl-carbamoyl O	Y214 O_{η}	99.0
L-Arg(1) N_{ε}	E144 $O_{\varepsilon 1}$	100.0
L-Arg(1) $N_{\eta 1}$	E144 $O_{\varepsilon 2}$	99.0
L-Arg(1) $N_{\eta 2}$	D215 $O_{\delta 2}$	84.0
L-Asp(3) $O_{\delta 1}$	W97 $N_{\varepsilon 1}$	95.0
Water-mediated H-bonding interactions between argifin and SmChiB		
L-Arg(1) O	R294 $N_{\eta 2}$	69.0
L-Arg(1) $N_{\eta 2}$	D215 $O_{\delta 2}$	12.0
L-Asp(3) $O_{\delta 1}$	N101 $O_{\delta 1}$	93.0
L-Asp(3) O	D316 $O_{\delta 2}$	83.0
L-Asp(4) $O_{\delta 1}$	D336 $O_{\delta 2}$	0.0
L-Asp(4) O	D336 $O_{\delta 2}$	0.0
Dipeptide 2	*Sm*ChiB	% Occupied
B: Dipeptide **2**–*Sm*ChiB complex		
*Direct H-bonding interactions between dipeptide **2** and SmChiB*		
Methyl-carbamoyl N	D142 $O_{\delta 2}$	70.0
Methyl-carbamoyl O	Y214 O_{η}	99.0
L-Arg(1) N_{ε}	E144 $O_{\varepsilon 1}$	100.0
L-Arg(1) $N_{\eta 1}$	E144 $O_{\varepsilon 2}$	100.0
L-Arg(1) $N_{\eta 2}$	D215 $O_{\delta 2}$	95.0
L-Arg(1) O	R294 $N_{\eta 2}$	76.0
*Water-mediated H-bonding interactions between dipeptide **2** and SmChiB*		
L-Arg(1) $N_{\eta 2}$	D215 $O_{\delta 2}$	5.0
L-Arg(1) N	R294 $N_{\eta 1}$	7.0
N-Methyl-L-Phe(2) O	D316 $O_{\delta 1}$ or $O_{\delta 2}$	84.0

Hydrogen-bonding analysis was performed using *ptraj* module. Cutoff distance between heavy atoms, 3.8 Å. Cutoff H-donor–acceptor angle, 35°.

Table 3
Energy contributions (kcal/mol) to the binding free energy of dipeptide **2**–*Sm*ChiB and argifin–*Sm*ChiB complexes[a]

Contribution	Dipeptide **2**–*Sm*ChiB complex	Argifin–*Sm*ChiB complex	Difference[j]
ΔE_{int}[b]	−0.04 (7.31)	0.07 (8.94)	−0.11
ΔE_{VDW}[c]	−35.97 (4.72)	−43.26 (5.55)	7.29
ΔE_{elec}[d]	−51.97 (6.89)	−9.19 (8.34)	−42.78
ΔG_{PB}[e]	61.24 (6.62)	22.42 (7.55)	38.82
ΔG_{np}[f]	−6.09 (0.26)	−6.91 (0.23)	0.82
$-T\Delta S$[g]	26.51 (8.41)	30.57 (8.25)	−4.06
$\Delta G_{elec+PB}$[h]	9.27 (3.18)	13.23 (3.49)	−3.96
ΔG_{bind}[i]	−6.32 (11.17)	−6.30 (12.07)	−0.02
Experiment	IC_{50} = 3.7 μM	IC_{50} = 6.4 μM (K_d = 33 μM)	

[a] Results are mean values from 100 (5 in the case of entropy contributions) snapshots. Values in parentheses are standard deviations.
[b] Internal contributions from bond, angle dihedral terms.
[c] Nonbonded van der Waals.
[d] Nonbonded electrostatics.
[e] Electrostatic component to solvation.
[f] Nonpolar component to solvation.
[g] Entropic contributions to binding.
[h] $\Delta G_{elec+PB} = \Delta E_{elec} + \Delta G_{PB}$.
[i] Total change of free energy in binding.
[j] Dipeptide **2**—Argifin.

static interaction energies with dipeptide **2**. All of these five residues were acidic amino acids, that is, aspartic acid and glutamic acid. Figure 7 shows the location of these residues in the dipeptide **2**–*Sm*ChiB complex, which were close to the binding site of dipeptide **2** and **1**. The net charge of dipeptide **2** is zero in solution, while that of **1** is −1 (Fig. 1). Based on these observations, dipeptide **2** could be considered to have improved the electrostatic interaction with the acidic residues of *Sm*ChiB by reducing the net negative charge of the molecule. Therefore, we conclude that dipeptide **2** was better optimized against *Sm*ChiB than **1** from an electrostatic point of view.

3. Conclusion

We used a combination of NMR experiments and computational methods to investigate the basis for dipeptide *N*-acetyl-Arg{N^{ω}-(*N*-methylcarbamoyl)}-*N*-methyl-Phe(**2**) to possess potent inhibitory activity against *Sm*ChiB compared with argifin (**1**). The TRNOE experiment and docking calculation indicated that **2** binds to *Sm*ChiB in a similar fashion to that observed for N^{ω}-(*N*-methylcarbamoyl)-Arg(1) and *N*-methyl-Phe(2) of argifin in the crystal structure of the argifin–*Sm*ChiB complex. The binding free energy calculations with the MM-PBSA method considering water-mediated interactions suggested that both **1** and **2** bind to *Sm*ChiB with similar affinities, which is consistent with their experimental IC_{50} values. The van der Waals and nonpolar solvation energies of dipeptide **2** were less favorable than that of **1**. However, dipeptide **2** takes advantage of more favorable contributions of the total electrostatic component ($\Delta G_{elec+PB}$) and solute entropy to possess a binding affinity comparable with **1**. The binding of **2** with *Sm*ChiB resulted in a reduced tightening of the complex structure compared with **1** and, hence, a more favorable contribution of solute entropy. The improved total electrostatic component was derived from more favorable electrostatic interactions. Therefore, dipeptide **2** could be better optimized against *Sm*ChiB than **1** from an electrostatic point of view. The insights obtained herein might provide a general basis for the design of potent small-molecule inhibitors.

4. Materials and methods

4.1. NMR experiment

*Sm*ChiB was overexpressed in *Escherichia coli* and purified as previously described.[36] The preparation of dipeptide **2** was carried out by the efficient solid-phase synthesis strategy developed in our laboratory.[15] For NMR experiments, **2** was dissolved in 600 μl 0.1 M phosphate D_2O buffer (pH 7.0) to a final concentration of 1.5 mM. The dipeptide **2**-*Sm*ChiB complex NMR sample was prepared by dissolving **2** and *Sm*ChiB at concentrations of 1.5 mM and 0.05 mM, respectively, in 600 μl of D_2O buffer solution at a dipeptide **2**/*Sm*ChiB ratio of 30:1. High-resolution one-dimensional (1D) and two-dimensional (2D) ^{1}H NMR experiments were performed on a Varian INOVA600 spectrometer operating at a proton frequency of 600 MHz. All spectra were recorded at 37 °C. Water suppression was achieved by continuous low-power irradiation (2 s) during the relaxation delay with the transmitter frequency set on H_2O resonance. Two-dimensional DQF-COSY,[22] TOCSY,[23] ROESY,[24] and NOESY[25] were performed in the phase-sensitive mode.[37] DQF-COSY spectra were recorded with 512 increments of 4 K data points and 32 transients. NOESY experiments were carried out with mixing times of 100, 150, 200 and 250 ms. ROESY experiments were performed with mixing times of 200 ms. 256 increments of 2 K data points were recorded with 32–96 transients for TOCSY, NOESY and ROESY experiments.

4.2. Modeling of dipeptide 2–*Sm*ChiB complex

The initial three-dimensional (3D) structure of dipeptide **2** was constructed using ChemDraw Ultra 8.0 and Chem3D Ultra 8.0 (CambridgeSoft Corporation, Cambridge, MA) and translated into

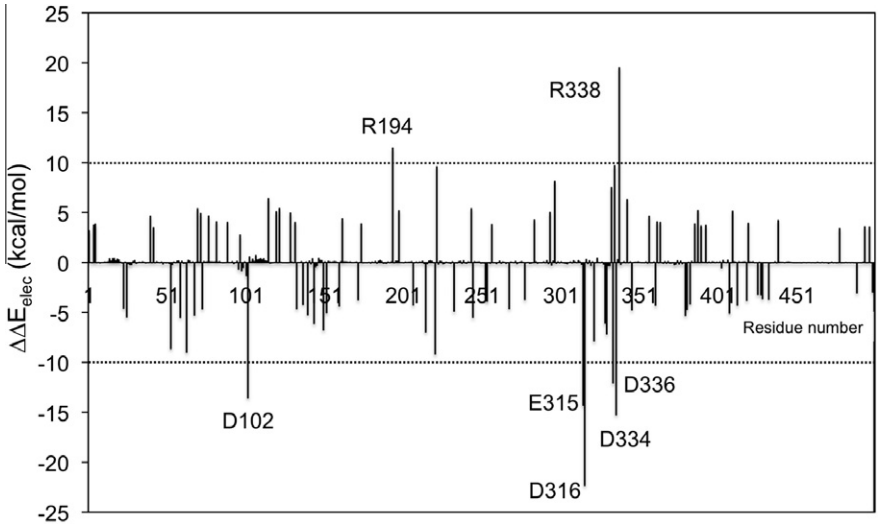

Figure 6. Distribution of difference of electrostatic interaction energies between dipeptide **2**–*Sm*ChiB complex and those of argifin–*Sm*ChiB complex. Residues with an absolute difference larger than 10.0 kcal/mol are labeled.

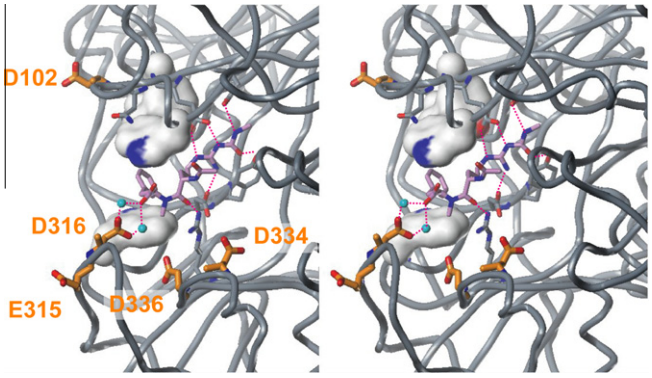

Figure 7. Stereoview of surroundings of dipeptide **2** binding site of *Sm*ChiB. Five acidic residues (D102, E315, D316, D334, and D336) colored orange.

Tripos Mol2 file (.mol2) format. Hypothetically hydrated ligand molecules for dipeptide **2** were then prepared by connecting ligand hydrogen-bonding functional groups with water molecules through a hypothetical bond of 2.7 Å (a typical distance for hydrogen bonding, Fig. 8).[20] In this preparation, the carbonyl (or carboxyl) and hydroxyl oxygen atoms were translated to sp2 and sp3 carbon atoms (C.2 and C.3 Sybyl atom types), respectively, which was intended for the future molecular design of novel inhibitors by incorporating water-mediated interactions.[20] These changes also aim to remove the hydrogen bonding ability of ligand oxygen atom connected to a water molecule during the docking calculation. We constructed the hypothetically hydrated ligand molecules with a maximum of two water molecules. As a result, we prepared a total of 46 molecular structures for the docking calculation of peptide **2**, which consisted of a native molecule not connected to water molecules, nine molecules connected to one water molecule, and 36 molecules connected to two water molecules (Supplementary Fig. 3).

The docking calculation of peptide **2** against *Sm*ChiB was performed by the SURFLEX-DOCK[38] program implemented in SYBYL 7.3.3 (Tripos, St. Louis, MO). The crystal structure of the argifin–*Sm*ChiB complex (PDB: 1H0I) was used to obtain the *Sm*ChiB template structure for docking. A total of 2300 different docking poses were generated, and each was evaluated using five different score functions: Surflex-Score,[38] D-Score,[39] G-Score,[40] ChemScore[41] and PMF-Score[42] implemented in the SYBYL CScore module. The AASS (Average of Auto-Scaled Scores)[43] index, recently defined in our laboratory to rank docking models more adequately, was then applied. The top 20 poses were selected, and each pose was restored to the native structure of peptide **2** and the water molecules (Supplementary Fig. 4A and B).

The top 20 poses were solvated in water droplets by applying the SYBYL SOLVENT command (Supplementary Fig. 4C), and refined through energy minimization for a region of 8 Å around docked peptide **2** using the Tripos force field. The partial atomic charges of *Sm*ChiB were obtained from AMBER parm94, and those of peptide **2** were obtained by the Gasteiger–Hückel method. A dielectric constant of 1 was used. After the energy minimization calculations, water molecules not involved in water-mediated interactions between ligands and proteins were removed. This enabled us to find additional potential water-mediated interactions (Supplementary Fig. 4D).

The resulting complex structures were subjected to MM-PBSA calculations using the SYBYL ZAP program.[44] Using the general MM-PBSA method,[21] the free energy of a molecule (G_{mol}) is calculated as follows:

$$G_{mol} = E_{gas} + G_{solv} - TS_{solute}. \quad (3)$$

Here, E_{gas}, G_{solv}, and $-TS_{solute}$ denote the total molecular mechanical (MM) energies of a molecule in the gas phase, its solvation free energy, and an estimate of the solute entropy, respectively. The $-TS_{solute}$ term was not included in this calculation. When comparing a number of poses obtained in the docking calculation between a protein and a ligand, however, we might reasonably assume that the contribution of the $-TS_{solute}$ term is relatively constant. Therefore, the free energies of complex structures ($G_{complex}$s) were approximated without the $-TS_{solute}$ term as follows:

$$G_{complex} \approx E_{gas} + G_{solv}. \quad (4)$$

E_{gas} includes the internal (E_{int}; i.e., bond, angle and dihedral), van der Waals (E_{VDW}), and electrostatic (E_{elec}) energies. It is calculated using the Tripos force field and the partial atomic charges used in the energy minimization described above. The solvation free energy is divided into two parts:

$$G_{solv} = G_{PB} + G_{np}. \quad (5)$$

G_{PB} and G_{np} are electrostatic and nonpolar contributions to the solvation free energy, respectively. They were calculated with the

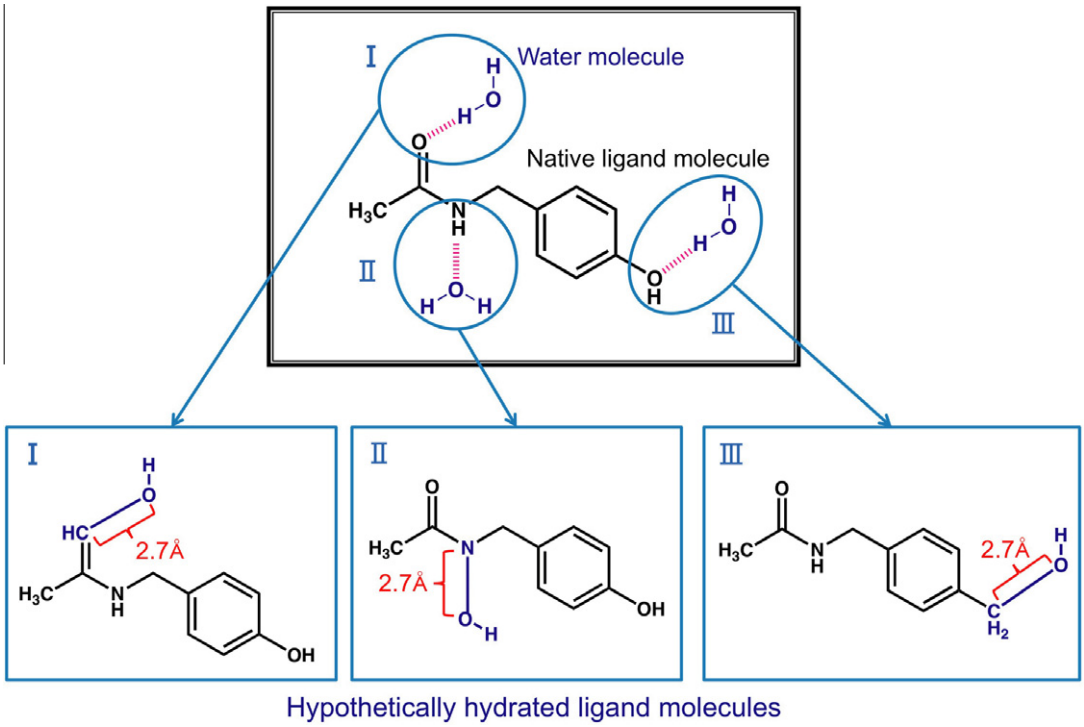

Figure 8. Preparation procedure of hypothetically hydrated ligand molecules.

SYBYL ZAP program. Dielectric constants of 2 and 80 were used for the interior and exterior, respectively. The dielectric boundary was taken as the solvent-accessible surface defined by a 1.4-Å probe radius. G_{np} was calculated using the solvent-accessible surface area (SASA), where $G_{np} = \gamma$ (SASA) + β (γ = 0.00542 kcal/[mol Å^2], β = 0.92 kcal/mol).[29] Finally, we selected a pose with the lowest $G_{complex}$ as the interaction model. The result of the MM-PBSA calculation for the top 20 poses is included in Supplementary Table 2. The top-ranked pose was shown to be more stable than the second by at least 2 kcal/mol.

4.3. MD simulations

All MD simulations presented herein were performed using the AMBER8.0 simulation package.[26] For consistency with our previous argifin–*Sm*ChiB complex study, we used the Cornell et al. force field[27] and the partial charges for peptide **2** derived from the restraint electrostatic potential (RESP) method using an ab initio calculation at the HF/6-31G* level.[28,45] The resulting structure of the peptide **2**–*Sm*ChiB complex was solvated in a box of TIP3P water molecules with a margin of 10 Å along each dimension. Four Na^+ ions were added to neutralize the system. The total number of atoms was 67,666.

Equilibration was carried out as follows: to relax the water around the solute, it was minimized for 1000 steps, followed by 35 ps of 310 K MD with 100 kcal/(mol Å^2) restraints on all solute atoms. This was followed by five rounds of 1000-step energy minimizations on the entire system. Harmonic constraints were applied to all heavy atoms with a strength of 100, 25, 5, 1 and 0 kcal/(mol Å^2) at each round. Finally, the system was heated from 0 to 310 K in 40 ps. After this equilibration phase, the production phase followed at 310 K for up to 3000 ps. The MD simulation was carried out at constant pressure (1 atm) and temperature (310 K), under periodic boundary conditions, and with particle-mesh Ewald treatment of electrostatics.[46] SHAKE[47] was applied to all bonds involving hydrogen, and a time step of 1 fs was used. An 8-Å cutoff was used for the nonbonded interactions.

The MD simulation of peptide **2** in its free state was performed to obtain its solution conformations. We constructed two different initial structures: one with a *cis*-configuration of the amide bond between N^{ω}-(*N*-methylcarbamoyl)-Arg(1) and *N*-methyl-Phe(2) and another with a *trans*-configuration. MD simulations using these two initial structures were performed using the conditions described above.

Hydrogen-bonding analysis of MD trajectories was performed using the *ptraj* module of AMBER8.0.[26] The cutoff distance between the heavy atoms was 3.8 Å, and the cutoff H-donor–acceptor angle was 35°.

4.4. Estimation of binding affinities by the MM-PBSA method using the MD trajectory

The binding free energy of peptide **2** to *Sm*ChiB was estimated as follows: a total of 100 snapshots were extracted from the last 1000 ps on the MD trajectory of the peptide **2**-*Sm*ChiB complex with an interval of 10 ps. As observed in Section 2, two water molecules involved in the hydrogen-bonding bridges between dipeptide **2** and *Sm*ChiB with high occupancy seem to play an important role in forming and stabilizing the complex structure (Fig. 5B). Therefore, these water molecules were explicitly retained, while other water and Na^+ molecules were removed from the snapshots. The above procedure led to a representative ensemble of the dipeptide **2**–*Sm*ChiB complex. The coordinates for unbound *Sm*ChiB were prepared by removing dipeptide **2** from the ensemble of complex structures. Water molecules involved in the hydrogen-bonding bridges were part of the protein. The unbound conformations of peptide **2** were obtained from two separate MD trajectories of free ligand in solution.

Utilizing these conformations taken from the MD simulations, $G_{complex}$, $G_{free\ protein}$ ($\approx G_{bound\ protein}$), and $G_{free\ ligand}$ were estimated using Eq. 3. $G_{free\ ligand}$ of **2** was estimated in the weighted-average manner according to the ratio from the NMR experiments. E_{gas} was calculated using the AMBER8.0 anal program without applying a cutoff for nonbonded interactions.[26] G_{PB} was estimated with the DELPHI

II program.[48] A dielectric constant of 80 was used for the solvent. On the other hand, three different dielectric constants of 1, 2 and 4 were examined for the interior. The MM-PBSA calculation using an interior dielectric constant of 2 could provide the value of binding free energy of argifin with *Sm*ChiB much closer to the experimental one. Therefore, the interior dielectric constant of 2 was also used for the peptide **2**–*Sm*ChiB complex. The radii of the atoms were taken from the PARSE parameter set.[49] G_{np} was calculated by applying the MSMS program[50] with a solvent probe radius of 1.4 Å. In this binding free energy calculation, the solute entropy ($-TS_{solute}$) was estimated using the normal-mode analysis. The structures of complex, unbound *Sm*ChiB, and unbound **2** were minimized with no cutoff for nonbonded interactions using the conjugate gradient and Newton–Raphson minimizations until the root-mean-square of the elements of the gradient vector was less than 10^{-4} kcal/(mol Å). Then, normal mode calculations were carried out with no cutoff for nonbonded interactions. A distance-dependent dielectric constant ($\varepsilon = 4R_{ij}$) was used to mimic solvent screening. Because this analysis required extensive computer time, only five snapshots were used to estimate the order of magnitude of the solute entropy. Finally, the absolute binding free energy (ΔG_{bind}) was estimated according to Eq. 1. The absolute binding free energy (ΔG_{bind}) is represented by the following equation:

$$\Delta G_{bind} = \Delta E_{int} + \Delta E_{VDW} + \Delta E_{elec} + \Delta G_{PB} + \Delta G_{np} - T\Delta S. \quad (6)$$

Here, ΔE_{int} is the ligand strain defined as the difference in internal energies (bond, angle and dihedral terms) between the conformation in the bound state and the conformation free in solution, the ΔE_{VDW} and ΔE_{elec} terms are the van der Waals and electrostatic interaction energies contributing to binding, respectively, the ΔG_{PB} and ΔG_{np} terms are the electrostatic (polar) and nonpolar contributions of solvation free energy to binding, respectively, and $-T\Delta S$ is the contribution of solute entropy to binding.

The binding free energy of **1** to *Sm*ChiB was also estimated using the MD trajectory obtained in our previous study.[28] Of note is that, unlike our previous study,[28] water molecules involved in the hydrogen-bonding bridges (Fig. 5A) were explicitly considered herein.

Acknowledgements

This work was supported, in part, by Grant-in-Aid for Scientific Research (C) of the Japan Society for the Promotion of Science [KAKENHI 21590046 (H.G.) and KAKENHI 18590015 (T.S.)], the Takeda Science Foundation, the Mochida Memorial Foundation for Medical and Pharmaceutical Research the Research Fellowships of the Japan Society for the Promotion of Science for Young Scientists (A.S.), and by the Kitasato University Research Grant for Young Researchers (H.G.). We also thank Mr. Toshiro Kimura (World Fusion Co., Ltd) for assistance with computational analysis.

Supplementary data

Supplementary data associated with this article can be found, in the online version, at doi:10.1016/j.bmc.2010.06.093. These data include MOL files and InChiKeys of the most important compounds described in this article.

References and notes

1. Brurberg, M. B.; Nes, I. F.; Eijsink, V. G. H. *Microbiology* **1996**, *142*, 1581.
2. Kuranda, M. J.; Robbins, P. W. *J. Biol. Chem.* **1991**, *266*, 19758.
3. Merzendorfer, H.; Zimoch, L. *J. Exp. Biol.* **2003**, *206*, 4393.
4. Renkema, G. H.; Boot, R. G.; Muijsers, A. O.; Donker-Koopman, W. E.; Aerts, J. M. F. G. *J. Biol. Chem.* **1995**, *270*, 2198.
5. Boot, R. G.; Blommaart, E. F. C.; Swart, E.; Ghauharali-van der Vlugt, K.; Bijl, N.; Moe, C.; Place, A.; Aerts, J. M. F. G. *J. Biol. Chem.* **2001**, *276*, 6770.
6. Takaya, N.; Yamazaki, D.; Horiuchi, H.; Ohta, A.; Takagi, M. *Biosci. Biotechnol. Biochem.* **1998**, *62*, 60.
7. Cohen, E. *Arch. Insect. Biochem. Physiol.* **1993**, *22*, 245.
8. Zhu, Z.; Zheng, T.; Homer, R. J.; Kim, Y. K.; Chen, N. Y.; Cohn, L.; Hamid, Q.; Elias, J. A. *Science* **2004**, *304*, 1678.
9. Kawada, M.; Hachiya, Y.; Arihiro, A.; Mizoguchi, E. *Keio J. Med.* **2007**, *56*, 21.
10. Shiomi, K.; Arai, N.; Iwai, Y.; Turberg, A.; Kölbl, H.; Ōmura, S. *Tetrahedron Lett.* **2000**, *41*, 2141.
11. Izumida, H.; Nishijima, M.; Takadera, T.; Nomoto, A. M.; Sano, H. *J. Antibiot.* **1996**, *49*, 829.
12. Ōmura, S.; Arai, N.; Yamaguchi, Y.; Masuma, R.; Iwai, Y.; Namikoshi, M.; Turberg, A.; Kölbl, H.; Shiomi, K. *J. Antibiot.* **2000**, *53*, 603.
13. Arai, N.; Shiomi, K.; Yamaguchi, Y.; Masuma, R.; Iwai, Y.; Turberg, A.; Kölbl, H.; Ōmura, S. *Chem. Pharm. Bull.* **2000**, *48*, 1442.
14. Dixon, M. J.; Andersen, O. A.; van Aalten, D. M.; Eggleston, I. M. *Bioorg. Med. Chem. Lett.* **2005**, *15*, 4717.
15. Sunazuka, T.; Sugawara, A.; Iguchi, K.; Hirose, T.; Nagai, K.; Noguchi, Y.; Saito, Y.; Yamamoto, T.; Ui, H.; Gouda, H.; Shiomi, K.; Watanabe, T.; Ōmura, S. *Bioorg. Med. Chem.* **2009**, *17*, 2751.
16. Houston, D. R.; Shiomi, K.; Arai, N.; Ōmura, S.; Peter, M. G.; Turberg, A.; Synstad, B.; Eijsink, V. G. H.; van Aalten, D. M. F. *Proc. Natl. Acad. Sci. U.S.A.* **2002**, *99*, 9127.
17. Clore, G. M.; Gronenborn, A. M. *J. Magn. Reson.* **1982**, *48*, 402.
18. Kim, J. I.; Nagano, T.; Higuchi, T.; Hirobe, M.; Shimada, I.; Arata, Y. *J. Am. Chem. Soc.* **1991**, *113*, 9392.
19. Radwan, A. A.; Gouda, H.; Yamaotsu, N.; Torigoe, H.; Hirono, S. *Drug Des. Discovery* **2001**, *17*, 265.
20. Genma, I.; Yamaotsu, N.; Sakoh, Y.; Gouda, H.; Hirono, S. Abstracts of the 35th Symposium of Structure–Activity Relationships, Ed. by the Division of Structure–Activity Studies, The Pharmaceutical Society of Japan, Tokyo, 2007, pp 115–118.
21. Kollman, P. A.; Massova, I.; Reyes, C.; Kuhn, B.; Huo, S.; Chong, L.; Lee, M.; Lee, T.; Duan, Y.; Wang, W.; Donini, O.; Cieplak, P.; Srinivasan, J.; Case, D. A.; Cheatham, T. E., III *Acc. Chem. Res.* **2000**, *33*, 889.
22. Rance, M.; Sørensen, O. W.; Bodenhausen, G.; Wagner, G.; Ernst, R. R.; Wuthrich, K. *Biochem. Biophys. Res. Commun.* **1983**, *117*, 479.
23. Bax, A.; Davis, D. G. *J. Magn. Reson.* **1985**, *65*, 355.
24. Bax, A.; Davis, D. G. *J. Magn. Reson.* **1985**, *63*, 207.
25. Macura, S.; Huang, Y.; Suter, D.; Ernst, R. R. *J. Magn. Reson.* **1981**, *43*, 259.
26. Case, D. A.; Darden, T. A.; Cheatham, T. E., III; Simmerling, C. L.; Wang, J.; Duke, R. E.; Luo, R.; Merz, K. M.; Wang, B.; Pearlman, D. A.; Crowley, M.; Brozell, S.; Tsui, V.; Gohlke, H.; Mongan, J.; Hornak, V.; Cui, G.; Beroza, P.; Schafmeister, C.; Caldwell, J. W.; Ross, W. S.; Kollman, P. A. AMBER8; University of California: San Francisco, 2004.
27. Cornell, W. D.; Cieplak, P.; Bayly, C. I.; Gould, I. R.; Merz, K. M., Jr.; Ferguson, D. M.; Spellmeyer, D. C.; Fox, T.; Caldwell, J. W.; Kollman, P. A. *J. Am. Chem. Soc.* **1995**, *117*, 5179.
28. Gouda, H.; Yanai, Y.; Sugawara, A.; Sunazuka, T.; Ōmura, S.; Hirono, S. *Bioorg. Med. Chem.* **2008**, *16*, 3565.
29. Massova, I.; Kollman, P. A. *J. Am. Chem. Soc.* **1999**, *121*, 8133.
30. Wang, W.; Lim, W. A.; Jakalian, A.; Wang, J.; Wang, J.; Luo, R.; Bayly, C. I.; Kollman, P. A. *J. Am. Chem. Soc.* **2001**, *123*, 3986.
31. Chong, L. T.; Duan, Y.; Wang, L.; Massova, I.; Kollman, P. A. *Proc. Natl. Acad. Sci. U.S.A.* **1999**, *96*, 14330.
32. Huo, S.; Wang, J.; Cieplak, P.; Kollman, P. A.; Kuntz, I. D. *J. Med. Chem.* **2002**, *45*, 1412.
33. Masukawa, K. M.; Kollman, P. A.; Kuntz, I. D. *J. Med. Chem.* **2003**, *46*, 5628.
34. Gouda, H.; Kuntz, I. D.; Case, D. A.; Kollman, P. A. *Biopolymers* **2003**, *68*, 16.
35. Spacková, N.; Cheatham, T. E., III; Ryjácek, F.; Lankas, F.; Van Meervelt, L.; Hobza, P.; Sponer, J. *J. Am. Chem. Soc.* **2003**, *125*, 1759.
36. Hirose, T.; Sunazuka, T.; Sugawara, A.; Endo, A.; Iguchi, K.; Yamamoto, T.; Ui, H.; Shiomi, K.; Watanabe, T.; Sharpless, K. B.; Ōmura, S. *J. Antibiot.* **2009**, *62*, 277.
37. States, D. J.; Haberkorn, R. A.; Ruben, D. J. *J. Magn. Reson.* **1982**, *48*, 286.
38. Jain, A. N. *J. Med. Chem.* **2003**, *46*, 499.
39. Kuntz, I. D.; Blaney, J. M.; Oatley, S. J.; Langridge, R.; Ferrin, T. E. *J. Mol. Biol.* **1982**, *161*, 269.
40. Jones, G.; Willett, P.; Glen, R. C.; Leach, A. R.; Taylor, R. *J. Mol. Biol.* **1997**, *267*, 727.
41. Eldridge, M. D.; Murray, C. W.; Auton, T. R.; Paolini, G. V.; Mee, R. P. *J. Comput. Aided Mol. Des.* **1997**, *11*, 425.
42. Muegge, I.; Martin, Y. C. *J. Med. Chem.* **1999**, *42*, 791.
43. Oda, A.; Tsuchida, K.; Takakura, T.; Yamaotsu, N.; Hirono, S. *J. Chem. Inf. Model.* **2006**, *46*, 380.
44. Grant, J. A.; .Pickup, B. T.; Nicholls, A. *J. Comput. Chem.* **2001**, *22*, 608.
45. Cieplak, P.; Cornel, W. D.; Bayly, C.; Kollman, P. A. *J. Comput. Chem.* **1995**, *16*, 1357.
46. Darden, T.; York, D.; Pedersen, L. *J. Chem. Phys.* **1993**, *98*, 10089.
47. Ryckaert, J. P.; Ciccotti, G.; Berendsen, H. J. C. *J. Comput. Phys.* **1977**, *23*, 327.
48. Honig, B.; Nicholls, A. *Science* **1995**, *268*, 1144.
49. Sitkoff, D.; Sharp, K. A.; Honig, B. *J. Phys. Chem.* **1994**, *98*, 1978.
50. Sanner, M. F.; Olson, A. J.; Spehner, J. C. *Biopolymers* **1996**, *38*, 305.